Quantum Pumping Driven by an AC-field in Graphene Field Effect Transistor

[1]Mina D. Asham, [2]Walid A. Zein, [2]Adel H. Phillips

[1]Faculty of Engineering, Benha University, Benha, Egypt.
[2]Faculty of Engineering, Ain-Shams University, Cairo, Egypt.
minadanial@yahoo.com, adel.phillips@gmail.com

Abstract: Spin dependent transport characteristics through normal graphene/ ferromagnetic graphene/ normal graphene junction is investigated. The conduction of this junction is derived by solving Dirac equation for both parallel and anti-parallel spin alignments of electrons. Numerical calculations are performed for the conductance for both spin alignments. Oscillatory behavior of the conductance for the two cases is due to the interplay between the photons of the induced AC-signal with both spin-up and spin-down subbands. These oscillations are due to the modulation of the Fermi energy by the potential of the magnetic insulator and photon-energy. Also, the calculations of spin polarization and giant magneto-resistance show that these parameters could be modified by the barrier height and the angle of incidence of electrons on the corresponding region of the present device. Quantum pumping by induction of external photons could enhance spin transport mechanism through such investigated device. The present results show that the cut-off frequency for both parallel and anti-parallel spin alignments varies strongly in the range of THz to 10^{19} Hz. The present investigation could be found for designing very high speed nano-electronic devices and applications in the field of nano-biotechnology, for example, imaging processing.
[Mina D. Asham, Walid A. Zein, Adel H. Phillips. **Quantum Pumping Driven by an AC-field in Graphene Field Effect Transistor.** *J Am Sci* 2012;8(7):374-381]. (ISSN: 1545-1003). http://www.jofamericanscience.org. 57

Keywords: Graphene Field-Effect Transistor (GFET), Spin Transport, AC-field, Cutoff frequency.
Corresponding author: Mina D. Asham, Adel H. Phillips.

1. Introduction

Spin polarized transport has attracted lots of attention because of its potential applications to spintronic devices (Zutic *et al.,* 2004). It is an important issue in spintronics that how to effectively control and manipulate the spin degree of freedom in solid state systems. In 2004, a single atomic layer of graphitic carbon, known as graphene, was isolated by the Geim group (Novoselov *et al.,* 2004). Graphene is a single two-dimensional array of carbon atoms packed into a honeycomb lattice (Novoselov *et al.,* 2004 and Novoselov *et al.,*2005). Shubnikov-deHaas oscillation measurements done on graphene show that the electrons in graphene behave like massless relativistic particles. The band structures or electronic dispersion for these particles exhibit two bands which intersect at the equivalent points *K* and *Ḱ* (Novoselov *et al.,* 2004, Novoselov *et al.,* 2005 and Castro Neto *et al.,* 2009). In a 2-dimensional momentum versus E (3D) plot, the band structure appears as two cones, a right side-up cone (bottom) for the holes and an inverted cone (top) for the electrons (Castro Neto *et al.,* 2009 and Mina *et al.,* 2012). The two points *K* and *Ḱ* are the so-called Dirac points. The cone-like dispersion relations are similar to the energy-momentum relation for the 2D-massless relativistic particles that are governed by the 2D-Dirac-Weyl equation (Beenakker *et al.,* 2008, Castro Neto *et al.,* 2009, Mina *et al.,* 2011 and Mina *et al.,* 2012). One of the most unexpected uses of graphene is in biological applications. The recent findings of graphene's ability to facilitate the differentiation of stem cells without interference of growth or alteration of the growth environment of the cells (Nayak *et al.,* 2011) have instigated more interest in graphene in the biomedical community. Not only that, the sensitive charge-carrier modulation of chemically modified graphene has allowed the development of bio-devices that can detect a single bacterium or that can sense DNA (Mohanty *et al.,* 2008). Also, graphene shows an interesting variety of applications in the field of sensors and actuators (Zhu *et al.,* 2011).

Graphene has high potential for spintronics applications due to its expected long spin relaxation length and long spin relaxation time (Hill *et al.,* 2006, Ertler *et al.,* 2009 and Jozsa *et al.,* 2009). The reasons for graphene's long spin relaxation time would be the weak hyperfine interaction and weak intrinsic spin-orbit coupling (Tombros *et al.,*2007). It is known that the graphene's ferromagnetism can be induced intrinsically (Kan *et al.,* 2007) or extrinsically (Han *et al.,* 2010), among which the former may come from the electron-electron interaction and the latter could be induced by the ferromagnetic proximity effect. For example, the exchange splitting in the graphene, caused by the ferromagnetic proximity effect of the ferromagnet insulator EuO, has been estimated to be about 5 meV (Haugen *et al.,* 2008). Spin polarized current through ferromagnetic graphene has been investigated by many authors (Kan *et al.,* 2007,

Semenov *et al.,* 2007, Bai *et al.,* 2008, Haugen *et al.,* 2008, Han *et al.,* 2010 and Michetti *et al.,* 2010).

The aim of the present paper is to investigate the spin-dependent transport characteristics through ferromagnetic graphene junction. The spin polarization of the Dirac fermions tunneled through such junction is pumped by the influence of an AC-field of wide range of frequencies.

2. Theoretical Model

In this section, we shall derive an expression for the conductance for the proposed spintronic device. The graphene-based such device is modeled as follows:

Spin transport in normal graphene/ ferromagnetic graphene/ normal graphene mesoscopic junction is shown in fig. (1). Graphene can be converted into ferromagnetic state by depositing the magnetic insulator EuO on top of it (Haugen *et al.,* 2008) (see region IV) and a metallic gate. While regions I, II III and V are normal graphene. On the top of region II, together with the metallic gate, there is a ferromagnetic vector potential barrier. With such construction of spintronic device, we can inject and manipulate spins of Dirac fermions as we shall see below.

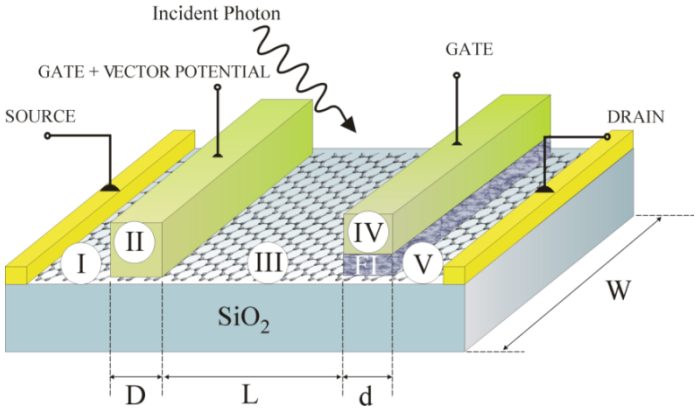

Figure 1 The proposed device model

The spin transport through the present investigated device is described by the following Dirac equation (Nomura *et al.,* 2007):

$$\left[\hbar v_F\left[\sigma_x k_x + \sigma_y\left(k_y - \frac{eA_y(x)}{\hbar}\right)\right] - [\sigma h(x) + U(x)]\sigma_o + eV_{ac}\cos\omega t\right]\psi = E\psi, \quad (1)$$

where v_F is the Fermi-velocity, σ_x & σ_y are the Pauli spin matrices, k_x & k_y are the wave vectors of the Dirac electrons in the x-y plane, $A_y(x)$ is the vector magnetic potential, $U(x)$ is the potential in the corresponding region, $\hbar$ is the reduced Planck's constant. The induced AC-field is described by the term $\{eV_{ac}\cos\omega t\}$, where V_{ac} is the amplitude of the AC-field, and ω is its frequency. In eq. (1), $h(x)$ is the position dependent of the exchange energy of the ferromagnetic graphene.

The solution of eq.(1) in one-dimension gives the following eign-functions in the corresponding regions are (Platero *et al.,* 2004 and Mina *et al.,* 2011):

$$\psi_I = \sum_{n=1}^{\infty}\left[\begin{pmatrix}1\\ e^{i\theta}\end{pmatrix}e^{ipx\cos\theta} + r\begin{pmatrix}1\\ -e^{-i\theta}\end{pmatrix}e^{-ipx\cos\theta}\right]\times J_n\left(\frac{eV_{ac}}{\hbar\omega}\right)e^{-in\omega t} \quad (2)$$

The eigen-function ψ_{II} in region II is:

$$\psi_{II} = \sum_{n=1}^{\infty}\left[a\begin{pmatrix}1\\ e^{i\theta_B}\end{pmatrix}e^{iqx\cos\theta_B} + b\begin{pmatrix}1\\ -e^{-i\theta_B}\end{pmatrix}e^{-iqx\cos\theta_B}\right]\times J_n\left(\frac{eV_{ac}}{\hbar\omega}\right)e^{-in\omega t} \quad (3)$$

The eigen-function ψ_{III} in region III is:

$$\psi_{III} = \sum_{n=1}^{\infty}\left[c\begin{pmatrix}1\\ e^{i\theta}\end{pmatrix}e^{ipx\cos\theta} + d\begin{pmatrix}1\\ -e^{-i\theta}\end{pmatrix}e^{-ipx\cos\theta}\right]\times J_n\left(\frac{eV_{ac}}{\hbar\omega}\right)e^{-in\omega t} \quad (4)$$

Also, the eigen-function ψ_{IV} in region IV is:

$$\psi_{IV} = \sum_{n=1}^{\infty}\left[f_1\begin{pmatrix}1\\ e^{i\theta_f}\end{pmatrix}e^{ikx\cos\theta_f} + f_2\begin{pmatrix}1\\ -e^{-i\theta_f}\end{pmatrix}e^{-ikx\cos\theta_f}\right]\times J_n\left(\frac{eV_{ac}}{\hbar\omega}\right)e^{-in\omega t} \quad (5)$$

And finally, the eigen-function ψ_V in region V is:

$$\psi_V = \sum_{n=1}^{\infty}\left[t\begin{pmatrix}1\\ e^{i\theta}\end{pmatrix}e^{ipx\cos\theta}\right]\times J_n\left(\frac{eV_{ac}}{\hbar\omega}\right)e^{-in\omega t} \quad (6)$$

where r & t are the reflection and transmission coefficients, and $J_n\left(\frac{eV_{ac}}{\hbar\omega}\right)$ is the n^{th} order of Bessel function of first kind and the solutions of eqs.(2, 3, 4, 5 & 6) must be generated by the presence of the different side-bands, "n", which comes with the phase factor $e^{-in\omega t}$ (Amin *et al.,* 2009, Mina *et al.,* 2011 and Zein *et al.,* 2011). In eqs. (2, 3, 4, 5 & 6), the following parameters are: the parameter θ is the angle of incidence on the normal graphene (regions I, III & V), the angle θ_B is the angle of incidence on the graphene (region II) and the angle θ_f is the angle of incidence on graphene (region IV). The parameters p, q & k are the wave vectors in the corresponding regions of graphene which are expressed as:

$$p = (E + eV_{sd} + E_F + n\hbar\omega)/\hbar v_F, \quad (7)$$

$$q = \begin{pmatrix} E + eV_{sd} + E_F + V_d + \\ \frac{1}{2} g\mu_B B\sigma_L + eV_g + n\hbar\omega \end{pmatrix}/\hbar v_F, \quad (8)$$

and

$$k = \begin{pmatrix} E + eV_{sd} + E_F + \acute{V}_d + \\ eV_g + n\hbar\omega + \sigma_R h_o \end{pmatrix}/\hbar v_F, \quad (9)$$

where V_{sd} is the bias voltage, E_F is the Fermi-energy, V_g is the gate voltage, h_o is the exchange energy of the ferromagnetic graphene, g is the Lande g-factor, μ_B is the Bohr magneton, B is the magnetic field. V_d and $\acute{V}_d$ are the magnetic barriers in regions (II, III) respectively. The angles θ_B and θ_f are expressed in terms of the wave vectors p, q & k (eqs. 7, 8 & 9) as:

$$\sin\theta_B = (|p|/|q|)\sin\theta - 1/(|q|l_B), \quad (10)$$

and

$$\sin\theta_f = (|p|/|k|)\sin\theta - 1/(|k|l_B), \quad (11)$$

where l_B is the magnetic length which is equal to

$$l_B = \sqrt{\hbar/eB} \quad (12)$$

Now, applying the boundary conditions at the interface of each of two neighbored regions (see fig. (1)), we get the tunneling probability, $\Gamma_{with\ photons}(E)$, of the tunneled Dirac electrons, which takes the following form:

$$\Gamma_{with\ photons}(E) = \sum_{n=1}^{\infty} J_n^2\left(\frac{eV_{ac}}{n\hbar\omega}\right) \cdot \Gamma_{without\ photons}(E), \quad (13)$$

where $\Gamma_{without\ photons}(E)$ is the tunneling probability without the induction of photons of the applied AC-field, which is given by:

$$\Gamma_{without\ photons}(E) = |t|^2 = \left|\frac{\cos^2\theta\cos\theta_B\cos\theta_f e^{-ip(D+L+d)\cos\theta}}{\alpha_1 e^{ipL\cos\theta_B} + \alpha_2\alpha_3 e^{-ipL\cos\theta_B}}\right|^2, \quad (14)$$

where α_1, α_2 & α_3 are respectively given as :

$$\alpha_1 = (\sin\theta - \sin\theta_B)(\sin\theta - \sin\theta_f)\sin(qD\cos\theta_B)\sin(kd\cos\theta_f), \quad (15)$$

$$\alpha_2 = \cos\theta\cos\theta_B\cos(qD\cos\theta_B) - i(1 - \sin\theta\sin\theta_B)\sin(qD\cos\theta_B), \quad (16)$$

and

$$\alpha_3 = \cos\theta\cos\theta_f\cos(kd\cos\theta_f) - i(1 - \sin\theta\sin\theta_f)\sin(kd\cos\theta_f) \quad (17)$$

where D, L and d represent, respectively, the thickness of the regions II, III and IV.

The spin-dependent conductance, $\boldsymbol{G}$, of the present studied spintronics devices could be determined for both parallel and anti-parallel spin alignments using the following equation (Haugen *et al.,* 2008, Yokoyama, 2008 and Han *et al.,* 2010):

$$G = \frac{2e^2}{h}\cdot\frac{k_F W}{\pi}\int_{E_F}^{E_F+n\hbar\omega} dE \int_0^{\pi/2} \Gamma_{with\ photons}(E)\cos\theta\, d\theta \cdot \left(-\frac{\partial f_{FD}}{\partial E}\right), \quad (18)$$

where W is the width of the graphene sheet, k_F is the Fermi wave vectors and $\left(-\frac{\partial f_{FD}}{\partial E}\right)$ is the first derivative of the Fermi-Dirac distributuin function which is expressed as:

$$\left(-\frac{\partial f_{FD}}{\partial E}\right) = (4k_B T)^{-1}\cdot\cosh^{-2}\left(\frac{E - E_F + n\hbar\omega}{2k_B T}\right), \quad (19)$$

in which k_B is the Boltzmann constant and T is the absolute temperature.

Now, the spin manipulation and detection could be achieved by determining both the spin polarization, SP, and giant magneto-resistance, GMR. These Parameters are related to the conductance, G, with parallel and anti-parallel spin alignments through the following equations (Haugen *et al.,* 2008, Yokoyama, 2008 and Mojarabian *et al.,* 2011):

$$SP = \frac{G_{\uparrow\uparrow} - G_{\uparrow\downarrow}}{G_{\uparrow\uparrow} + G_{\uparrow\downarrow}}, \quad (20)$$

and

$$GMR = \frac{G_{\uparrow\uparrow} - G_{\uparrow\downarrow}}{G_{\uparrow\uparrow}}, \qquad (21)$$

where $G_{\uparrow\uparrow}$ is the conductance in case of parallel spin alignments and $G_{\uparrow\downarrow}$ is the conductance in case of anti-parallel spin alignments. The subscripts $\uparrow$ & $\downarrow$ corresponds to spin-up and spin-down respectively.

It is interesting to calculate the cutoff frequency, ν_T, of the present studied nano-electronic device which is expressed in terms of the maximum conductance, , for both parallel and anti-parallel spins via the following equation (Manasreh, 2005):

$$\nu_T = \frac{G_{\max(\uparrow\uparrow/\uparrow\downarrow)}}{2\pi C}, \qquad (22)$$

where C is the total capacitance of the graphene-based present device, given by:

$$\frac{1}{C} = \frac{1}{C_e} + \frac{1}{C_Q}, \qquad (23)$$

where C_e is the electrostatic capacitance and C_Q is the quantum capacitance which are given by (Fang *et al.,* 2007):

$$C_e = \frac{\epsilon_{ox}}{t_{ox}}, \qquad (24)$$

and

$$C_Q = \frac{2e^2 k_B T}{\pi(\hbar v_F)^2} ln\left[2\left(1 + cosh\left(\frac{\acute{E}_F}{k_B T}\right)\right)\right], \qquad (25)$$

where ϵ_{ox} is the dielectric constant of insulator oxide, t_{ox} is the thickness of the insulator oxide, e is the electron charge, k_B is Boltzmann constant, T is the absolute temperature, $\hbar$ is the reduced Planck's constant, v_F is the Fermi-velocity. $\acute{E}_F$ is the modulated Fermi energy by the potential of the magnetic insulator EuO (region IV) (Bai *et al.,* 2008 , Haugen *et al.,* 2008 and Yokoyama, 2008) and the energy of the induced photons.

3. Results and Discussion

Numerical calculations are performed for the conductance, G, (eq.18) for both cases of parallel and anti-parallel alignment of spins of the tunneled Dirac fermions. The values of the following parameters are: the values of dimension of the present device are (see fig. 1): W = 100 nm, D = 2 nm, L = 5 nm and d = 2 nm. The other parameters, for example, the temperature T = 50 K, the bias voltage V_{sd} = -1 V, the magnetic barrier V_d in region III is 0.5 eV and the amplitude of the induced AC-signal is V_{ac} = 0.25 V. While the values of the following parameters are taken according to the case of parallel or anti-parallel spin alignment (Haugen *et al.,* 2008, Yokoyama, 2008 and Mojarabian *et al.,*2011). That is, for the parallel case, the exchange energy of the ferromagnetic graphene, h_o = 10 meV, magnetic field B = 2 T and magnetic barrier V_d = 0.5 eV (region II). For the anti-parallel case, h_o = 5 meV, B = 20 T, and V_d = 0.1 eV. The Lande g-factor for graphene, g = 4 (Das Sarma *et al.,* 2011), and the Fermi-energy, E_F, is calculated according to the following equation (Das Sarma *et al.,* 2011):

$$E_F = \hbar v_F k_B, \qquad (26)$$

where v_F is the Fermi velocity, $v_F \approx 10^6$ m/s and the Fermi wave vector, k_F, is related to the charge-carrier concentration, n, through the following equation (Das Sarma *et al.,* 2011):

$$k_F = (\pi n)^{1/2}, \qquad (27)$$

where $n \approx 0.36 \times 10^{12}$ cm^{-2} (Das Sarma *et al.,* 2011).

Now, the features of our results are:

1. Figs. (2a, b & c) show the variation of the conductance G with the gate voltage, V_g, at different values of the frequency, ν, of the induced AC-signal. We notice that the value of the conductance for both cases of parallel and anti-parallel spin alignment increases as the value of frequency, ν, of the induced AC-signal increases (see figs. 2a, b & c).
2. These results indicate that the spin transport through the present nano-device is enhanced by the energy of the induced photons (Platero *et al.,* 2004, Amin *et al.,* 2009, Yan *et al.,* 2010 and Awadallah *et al.,* 2011). Also, the oscillatory behavior of the conductance for both cases of spin alignments (see Figs. 2a, b & c), might be explained as follows:
3. When Dirac fermions pass through the ferromagnetic graphene, they split into sub-bands, one for spin-up and the other for spin-down. This splitting leads to the conductance of the present device to be spin-dependent. This oscillatory behavior of the spin-dependent conductance is due to the interplay between the frequency of the induced AC-signal with both spin-up and spin-down sub-bands (Platero *et al.,* 2004, Amin *et al.,* 2009, Awadallah *et al.,* 2011 and Mina *et al.,* 2011). Also, as pointed out by many authors (Bai *et al.,* 2008, Haugen *et al.,* 2008, and Yokoyama, 2008) that these oscillations of the conductance are due to the modulation of the Fermi energy by the potential of the magnetic insulator EuO (region IV) and the energy of the induced photons.

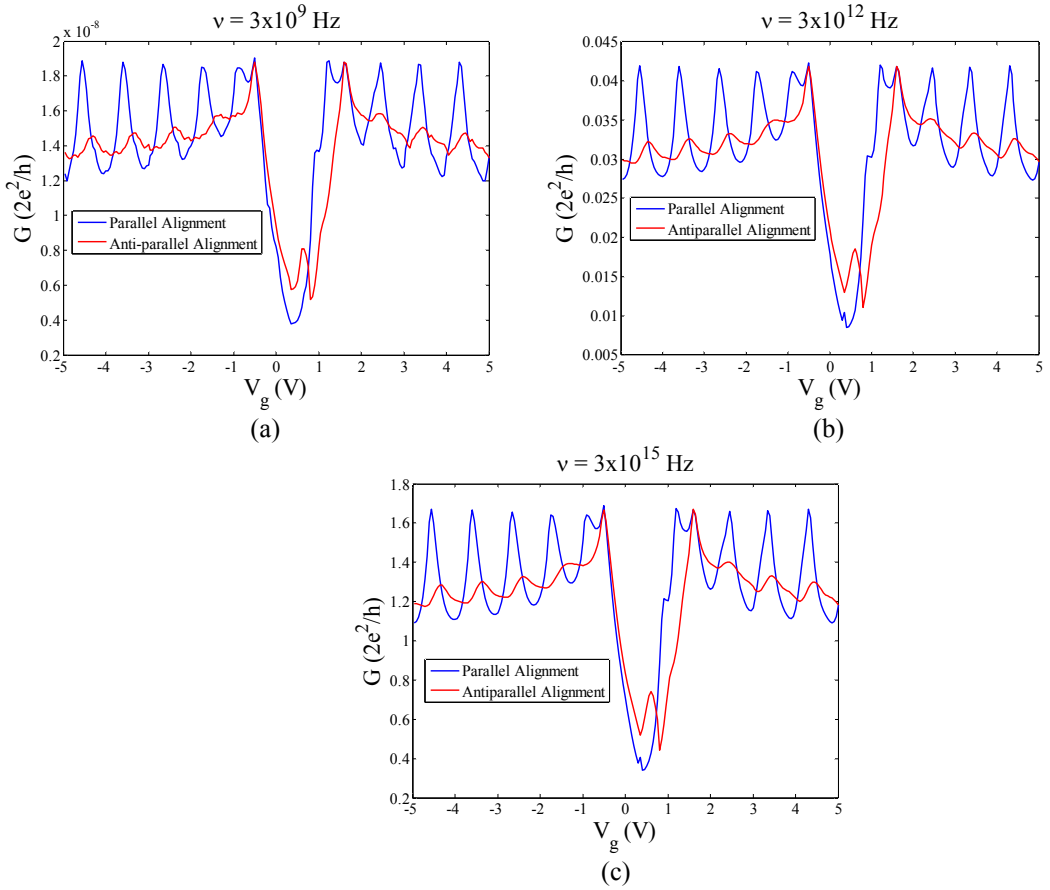

Figure 2 The variation of conductance G with the gate voltage V_g at frequencies ν = (a) $3x10^9$ Hz, (b) $3x10^{12}$ Hz, (c) $3x10^{15}$ Hz, for both spin alignments, parallel and anti-parallel.

4. Figs. (3 & 4) show the variation of the spin polarization, SP, and giant magneto-resistance, GMR, with the frequency of the induced photons at different values of the gate voltage. For V_g = 1.2 V, the spin polarization attains a maximum value ≈ 92.19 % and the corresponding giant magneto-resistance has a maximum value ≈ 95.94 % when $\nu = 3 \times 10^{10}$ Hz. While when the gate voltage, V_g, equals 0.85 V, the maximum values for SP and GMR are 41.21 % and 58.36 % respectively at $\nu = 3\times10^{11}$ Hz. For higher frequencies of the induced AC-signal, we notice that both spin polarization, SP, and giant magneto-resistance, GMR, are approximately constant for both values of V_g. The observed results in the present paper indicate that both spin polarization, SP, and giant magneto-resistance, GMR, can be modified not only by the barriers heights but also by the incident angles of the electron on the corresponding region of the present investigated device (Haugen *et al.,* 2008, Yokoyama, 2008, Yan *et al.,* 2010, Das Sarma *et al.,* 2011, Mina *et al.,* 2011 and Mojarabian *et al.,* 2011). The effect of induced photons is to enhance spin transport mechanism through the device (Platero *et al.,* 2004, Yan *et al.,* 2010 and Awadallah *et al.,* 2011).

So, we can point out that by adjusting another values of the barriers height and the incident angles, we may get another trend for both spin polarization and giant magneto-resistance. This is due to that quantum tunneling in graphene, is highly anisotropic due to the chiral nature of the Dirac fermion quasi-particles (Das Sarma *et al.,* 2011).

Figs. (5a, b & c) show the variation of the cutoff frequency, ν_T, with the gate voltage for both parallel and anti-parallel spin alignments. The calculations are performed for the three frequencies of the induced photons ($\nu = 3\times10^9$ Hz, 3×10^{12} Hz, 3×10^{15} Hz). From these figures, we notice the following:

a. The cutoff frequency, ν_T, for both spin alignments attains a maximum value $\nu_{Tmax} \approx 1.078\times10^{12}$ at $V_g \approx$ -0.5 V, when the frequency of the induced photon is $\nu = 3\times10^9$ Hz.
b. For $\nu = 3\times10^{12}$ Hz, the maximum value of the cutoff, ν_T, for both spin alignments is equal to $\nu_{Tmax} \approx 2.366\times10^{18}$ at $V_g \approx$ -0.5 V.
c. Also, for $\nu = 3\times10^{15}$ Hz, $\nu_{Tmax} \approx 9.426\times10^{19}$ Hz at $V_g \approx$ -0.5 V.

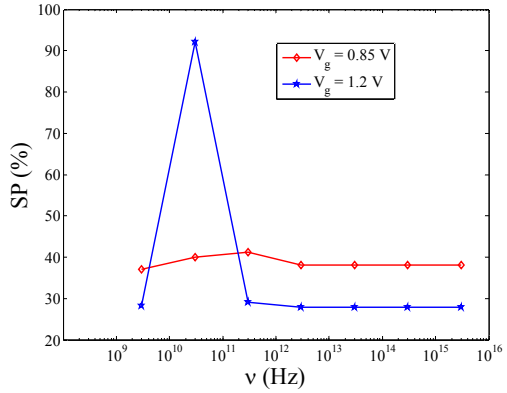

Figure 3 The spin polarization (SP) as a function of frequency ν at two different values of the gate voltage Vg = 0.85 V and 1.2 V.

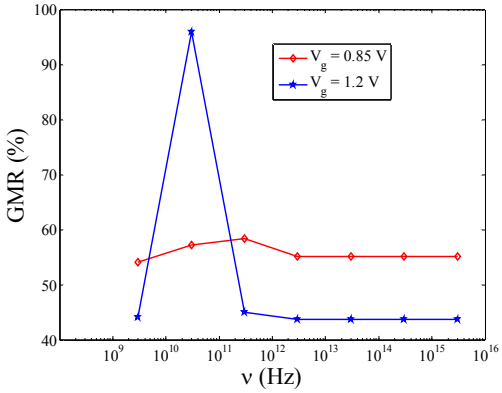

Figure 4 The giant magneto-resistance (GMR) as a function of frequency ν at two different values of the gate voltage V_g = 0.85 V and 1.2 V.

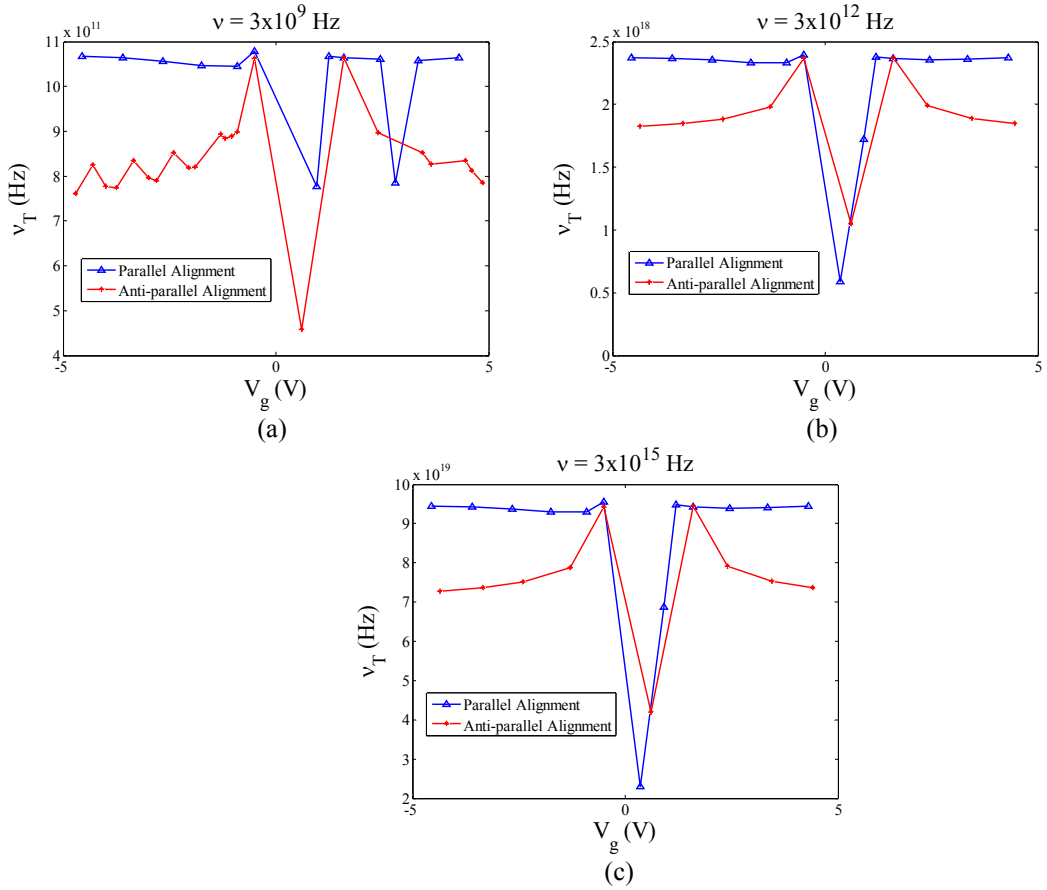

Figure 5 The variation of the cutoff frequency ν_T with the gate voltage V_g at frequencies ν = (a) 3x10^9 Hz, (b) 3x10^12 Hz, (c) 3x10^15 Hz, for both spin alignments, parallel and anti-parallel.

The authors (Liao *et al.,* 2010,Xia *et al.,* 2010, Chauhan *et al.,* 2011 & Wu *et al.,* 2011) examined the issue of ultimate channel length scaling for boosting the performance of graphene field effect transistor. They found that the cutoff frequency increases from the range GHz to THz as the channel length decreases.

In the present paper, the results for the cutoff frequency increases strongly from 10^{12} Hz up to 10^{19} Hz (see Figs.(5a, b & c)). These results might be explained as follows:

According to the structure of the present investigated nano-device, the channel length is affected by the external magnetic field, that is, we must take into account the magnetic length, l_B. The second parameter is the barrier heights and the modulation of the Fermi-energy by the potential of the magnetic insulator EuO. Also, the interplay between the frequency of the induced photons with both spin-up and spin-down sub-bands plays a role in computing the cutoff frequency.

4. Conclusion

Spin transport characteristics through normal graphene/ ferromagnetic graphene/ normal graphene junction is investigated. The effect of photon energy of the induced AC-signal is taken into consideration. The conductance is derived by solving Dirac equation. The computation of conductance corresponding to parallel and anti-parallel spin alignment and the corresponding spin polarization and giant magneto-resistance are performed. Also, the cutoff frequency is computed. The present results are found concordant with those in the literatures.

The present investigated junction could be applied in the field of nano-electronics, quantum information processing and in nano-biotechnology, for example, imaging processing.

References

1. Zutic I., Fabian J., Das Sarma S., 2004. Spintronics: Fundamentals and Applications. Review of Modern Physics; 76: 323.
2. Novoselov K. S., Geim A. K., Morozov S. V., Jiang D., Zhang Y., Dubonos S. V., Grigorieva I. V. Firsov A. A., 2004. Electric field effect in atomically thin carbon films. Science; 306: 666.
3. Novoselov K.S., Geim A. K., Morozov S. V., Jiang D., Katsnelson M. I., Dubonos S. V., Firsov A. A. ,2005. Two-dimensional gas of massless Dirac fermions in graphene. Nature; 438: 197.
4. Castro Neto A. H., Guinea F., Peres N. M. R., Novoselov K. S., Geim A. K., 2009. The electronic properties of graphene. Review of Modern Physics; 81: 109.
5. Mina A. N., Awadallah A. A., Phillips A. H., Ahmed R. R., 2012. Simulation of the band structure of graphene and carbon nanotube. Journal of Physics Conference series; 343: 012076.
6. Beenakker C. W. J., 2008. Andreev reflection and Klein tunneling in graphene. Review of Modern Physics; 80: 1337.
7. Mina A. N., Phillips A. H., 2011. Photon-assisted resonant chiral tunneling through a bilayer graphene barrier. Progress in Physics; 1: 112.
8. Nayak T. R., Andersen H., Makam V. S., Khaw C., Bae S., Xu X., Ee P. L. R., Ahn J. H., Hang B. H., Pastorin G., Ozyilmaz B. , 2011. Graphene for controlled and accelerated osteogenic differentiation of human mesenchymal stem cells. ACS Nano; 5: 4670.
9. Mohanty N., Berry V., 2008. Graphene single bacterium resolution bio-device and DNA transistor: Interfacing graphene derivatives with nanoscale and microscale biocomponents. Nano Letters; 8: 4469.
10. Zhu S. E., Shabani R., Rho J., Kim Y., Hang B. H., Ahn J. H., Cho H. J. , 2011. Graphene-based bio-morph-micro actuators. Nano Letters; 11: 977.
11. Hill E. W., Geim A. K., Novoselov K. S., Schedin F., Blake P., 2006. Graphene spin valve devices. IEEE Transactions on Magnetism; 42: 2694.
12. Jozsa C., Moasen T., Popinciuc M., Zomer P. j., Veligura A., Jonkman H. T., Van Wees B. J., 2009. Linear scaling between momentum and spin scattering in graphene. Physical Review B; 80: 241403.
13. Ertler C., Kanschuh S., Gmitra M., Fabian J., 2009. Electron spin relaxation in graphene: the role of substrate. Physical Review B; 80: 041405.
14. Tombros N., Jozsa C., Popinciuc M., Jonkman H. T., Van Wees B. J. , 2007. Electronic spin transport and spin precession in single graphene layers at room temperatures. Nature; 448: 571.
15. Kan E. J., Li Z., Yang J., Hou. J. G., 2007. Will zigzag graphene nanoribbon turn to half metal under electric field? Applied Physics Letters; 91: 243116.
16. Han W., Pi K., McCreary K. M., Li Y., Wong J. J. I., Swartz A. G., Kawakami R. K., 2010. Tunneling spin injection into single layer graphene. Physical Review Letters; 105: 167202.
17. Haugen H., Huertas-Hernando D., Brataas A., 2008. Spin transport in proximity-induced ferromagnetic graphene. Physical Review B; 77: 115406.
18. Bai C., Zhang X., 2008. Large oscillating tunnel magneto-resistance in ferro-magnetic graphene single tunnel junction. Physics Letters A; 372: 725.
19. Semenov Y. G., Kim K. W. Zavada J. M., 2007. Spin field effect transistor with a graphene channel. Applied Physics Letters; 91: 153105.
20. Michetti P., Recher P., Iannaccone G., 2010. Electric field control of spin rotation in bilayer graphene. Nano Letters; 10:4463.

21. Nomura K., McDonald A. H., 2007. Quantum transport of massless Dirac fermions. Physical Review Letters; 98: 076602.
22. Platero G. Aguado R., 2004. Photon-assisted transport in semiconductor nano-structures. Physics Reports; 395: 1-157.
23. Amin A. F., Li G. Q., Phillips A. H., Kleinekathofer U., 2009. Coherent control; of the spin current through quantum dot. European Physical Journal B; 68: 103.
24. Zein W. A., Ibrahim N. A., Phillips A. H. , 2011. Spin polarized transport in an AC-driven quantum curved nanowire. Physics Research International; ID-505091: 5 pages.
25. Yokoyama T., 2008. Controllable spin transport in ferromagnetic graphene junctions. Physical Review B; 77: 073413.
26. Mojarabian F. M., Rashedi G., 2011. GMR effects in graphene-based ferromagnetic/ normal/ ferromagnetic junctions. Physica E; 44: 647-653.
27. Manasreh O., 2005. Semiconductor hetero-junctions and nano-structures. McGraw-Hill.
28. Fang T., Konar A., Xing H., Jena D. , 2007. Carrier statistics and quantum capacitance of graphene sheets and ribbons. Applied Physics Letters; 91: 092109.
29. Das Sarma S., Adam S., Hwang E. H., Rossi E. , 2011. Electronic transport in two-dimensional graphene. Review of Modern Physics; 83: 407-470.
30. Awadallah A. A., Phillips A. H., Mina A. N., Ahmed R. R. ,2011. Photo-assisted transport in carbon nanotube meso-scopic device. International Journal of Nanoscience; 10(3): 419.
31. Yan C. H., Wei L. F., 2010. Tunneling of Dirac particles across graphene junctions bilaterally driven by AC-signals. Physica B; 405: 3995-3999.
32. Liao L., Bai J., Cheng R., Lin Y., Jiang S., Qu Y., Huang Y., Duan X., 2010. Sub-100 nm channel length graphene transistors. Nano Letters; 10: 3952-3956.
33. Xia F., Farmer D. B., Lin Y.-M., Avouris Ph., 2010. Field effect transistors with high on/off current ratio and large transport band gap at room temperature. Nano Letters; 10: 715-718.
34. Chauhan J., Guo J., 2011. Assessment of high frequency performance limits of graphene field-effect transistors. Nano Research; 4(6): 571-579.
35. Wu Y., Lin Y.-M., Bol A. A., Jenkins K. A., Xia F., Farmer D. B., Zhu Y. Avouris Ph., 2011. High frequency, scaled graphene transistors on diamond-like carbon. Nature; 472: 74-78.

6/10/2012